DMD Fast Forward. Published on June 24, 2011 as doi:10.1124/dmd.111.040873

DMD# 40873

Characterization and crystallization of mouse Aldehyde Oxidase 3 (mAOX3): from mouse liver to *E. coli* heterologous protein expression

Martin Mahro[*], Catarina Coelho[*], José Trincão, David Rodrigues, Mineko Terao, Enrico Garattini, Miguel Saggu, Friedhelm Lendzian, Peter Hildebrandt, Maria João Romão[†] and Silke Leimkühler[†]

Universität Potsdam, Institut für Biochemie and Biologie, Potsdam, Germany (M.M., S.L.), REQUIMTE, Departamento de Química, Faculdade de Ciências e Tecnologia, Universidade Nova de Lisboa, P-2829-516 Caparica, Portugal (C.C., J.T., D.R., M.J.R), Laboratory of Molecular Biology, Department of Biochemistry and Molecular Pharmacology, Istituto di Ricerche Farmacologiche Mario Negri, via La Masa 19, I-20156 Milano, Italy (M.T., E.G.); Technische Universität Berlin, Institut für Chemie, Sekr. PC14, Straße des 17 Juni 135, D-10623 Berlin, Germany (M.S., F.L., P.H.).

DMD Fast Forward. Published on June 24, 2011 as DOI: 10.1124/dmd.111.040873
This article has not been copyedited and formatted. The final version may differ from this version.

Running Title: Characterization and crystallization of mouse aldehyde oxidase 3

† *Corresponding authors:*

Silke Leimkühler, Universität Potsdam, Institut für Biochemie and Biologie, Potsdam, Germany, Tel: +49-331-977-5603, Fax: +49-331-977-5128,

E-mail: sleim@uni-potsdam.de

Maria João Romão, REQUIMTE, Departamento de Química, Faculdade de Ciências e Tecnologia, Universidade Nova de Lisboa, P-2829-516 Caparica, Portugal, Tel: +351-212948300, Fax: +351-212948550

E-mail: mromão@dq.fct.unl.pt

Text Pages (including references): 22

Tables: 5

Figures: 7

References: 32

Abstract : 233

Introduction : 684

Discussion : 391

Abbreviations: AOX3: aldehyde oxidase 3; AO: aldehyde oxidase; XOR: xanthine oxidoreductase; XO: xanthine oxidase; XDH: xanthine dehydrogenase; Moco: molybdopterin cofactor; *E. coli*: *Escherichia coli*; MCSF: moco sulfurase; DTT: dithiotreitol.

DMD Fast Forward. Published on June 24, 2011 as DOI: 10.1124/dmd.111.040873
This article has not been copyedited and formatted. The final version may differ from this version.

Abstract

Aldehyde oxidase (AOX) is characterized by a broad substrate specificity oxidizing aromatic aza-heterocycles, e.g. N^1-methylnicotinamide and N-methylphthalazinium, or aldehydes, such as benzaldehyde, retinal and vanillin. In the past decade, AO has been increasingly recognized to play an important role in the metabolism of drugs through its complex cofactor content, tissue distribution and substrate recognition. In humans, only one AOX gene (*AOX1*) is present, but in mouse and other mammals different AOX homologues were identified. The multiple AOX isoforms are expressed tissue-specifically in different organisms, and it is believed that they recognize distinct substrates and carry out different physiological tasks. AOX is a dimer of approximately 300 kDa, and each subunit of the homodimeric enzyme contains four different cofactors: the molybdenum cofactor (Moco), two distinct [2Fe-2S] clusters and one FAD. We purified the AOX homologue (mAOX3) from mouse liver and established a system for the heterologous expression of mAOX3 in *Escherichia coli*. The purified enzymes were compared. Both proteins show the same characteristics and catalytic properties, with the difference that the recombinant protein was expressed and purified in a 30% active form, while the native protein is 100% active. Spectroscopic characterizations showed that the FeSII is not completely assembled in mAOX3. Additionally, both proteins were crystallized. The best crystals were from the native mAOX3 and diffracted beyond 2.9Å. The crystals belong to space group P1 and two dimers are present in the unit cell.

DMD Fast Forward. Published on June 24, 2011 as DOI: 10.1124/dmd.111.040873
This article has not been copyedited and formatted. The final version may differ from this version.

Introduction

Aldehyde oxidase (AOX) is a complex molybdoflavoprotein that belongs to a family of structurally related molybdoenzymes, which bind the molybdenum cofactor (Moco) (Hille, 1996). AOX is homologous to xanthine oxidoreductase (XOR), another mammalian molybdoflavoenzyme, and both AOX and XOR show a remarkable degree of sequence similarity (Krenitsky, 1978, Garattini, *et al.*, 2003). AOX is active as a homodimer and each 150 kDa monomer consists of three separate domains that bind different cofactors: the 20 kDa N-terminal domain binds two distinct [2Fe-2S] clusters, the 40 kDa central domain binds the FAD cofactor, and the 80 kDa C-terminal domain binds Moco (Garattini, *et al.*, 2008). Moco-containing enzymes are further divided into three different families: the xanthine oxidase (XO) family, the sulfite oxidase (SO) family and the dimethylsulfoxide (DMSO) reductase family, which are classified in accordance to the ligands at the molybdenum active site (Hille, 1996).

Members of the XOR family are characterized by an equatorial sulfur ligand at the Moco, essential for enzyme activity (Wahl & Rajagopalan, 1982). Given the similarity in overall structures and subunit composition of AOX and XOR, the properties of the two enzymes are closely related. Both enzymes are present in the cytosol and are found in all vertebrates (Garattini, *et al.*, 2003). The primary difference, however, is that XOR can exist in two interconvertible forms, the xanthine oxidase (XO) and the xanthine dehydrogenase (XDH) (Nishino, *et al.*, 2008), while aldehyde oxidase solely exists in the oxidase form. AOX utilizes only molecular oxygen as the electron acceptor, in contrast to XOR, which transfers electrons to NAD^+ and to oxygen in the XDH and in the XO form, respectively. Notably, the substrate and inhibitor specificities of XOR and AOX differ, and in general AOX has

the ability to oxidize a broader range of substrates than XOR (Krenitsky, *et al.*, 1972). Typical substrates for AOX are compounds containing an aldehyde function, nitro/nitroso compounds, or *N*-heterocycles (Pryde, *et al.*, 2010). The biochemical and physiological functions of AOX in humans are still largely obscure. Single monogenic deficits for any AOX have not been described so far in mammalia, however, AOX is not essential for humans since genetic deficiencies in the Moco sulfurase (MCSF) gene are not associated with pathophysiological consequences. The ability of AOX to oxidize *N*-heterocycles makes it an important enzyme in the metabolism of drugs and xenobiotics (Pryde, *et al.*, 2010). In animals, AOX is likely to detoxify exogenously derived non-physiological compounds of wide structural diversity, and it is believed that the absence of AOX leads to symptoms under unusual circumstances of high intake of such xenobiotics. In humans, only one gene for AOX exists, while in mice and other mammals, different homologues of AOX were identified (Garattini, *et al.*, 2003). Since the identified proteins are highly homologous with the originally known aldehyde oxidase (named AOX1, the first vertebrate AO identified and characterized), the three related proteins are currently known as AOX3, AOX4 and AOX3L1 (formerly, AOH1, AOH2 and AOH3, respectively) (Garattini, *et al.*, 2003, Terao, *et al.*, 2006, Garattini & Terao, 2011). These multiple AOX isoforms are expressed tissue-specifically in different organisms, but their existence and expression pattern varies in different animal species (Garattini, *et al.*, 2003, Terao, *et al.*, 2006). It is believed that the various AOX isoforms recognize distinct substrates and carry out different physiological tasks.

The best studied AOX homologues are the ones identified in mouse. The tissue distribution of mouse AOX3 (mAOX3) is superimposable to that of mAOX1, and the two enzymes are predominantly synthesized in hepatic, lung, and testicular tissues

(Vila, *et al.*, 2004). Therefore, the comparison of the enzymatic properties of mAOX3 and mAOX1 is particularly relevant but has so far been very difficult (Terao, *et al.*, 2001).

Here, we established a reproducible system for the expression of mAOX3 in *E. coli* in a 30% functional form. The recombinant protein was compared in detail to the native protein purified from mouse liver as to its kinetic and spectroscopic properties. It was shown that both proteins had similar properties although, in comparison to mAOX1, the FeSII saturation was lower. The heterologous expression system for mAOX3 provided us with enough material to perform broad crystallization screenings. The vast majority of the crystallization trials were performed using the recombinant protein, and the crystallization conditions obtained were used to reproduce crystals using the native mAOX3 protein purified from mouse livers. We were able to obtain a usable dataset to 2.9 Å resolution with native mAOX3 crystals.

DMD Fast Forward. Published on June 24, 2011 as DOI: 10.1124/dmd.111.040873
This article has not been copyedited and formatted. The final version may differ from this version.

Materials and Methods

Bacterial Strains, Plasmids and Growth Conditions

E.coli TP1000 (Δ*mobAB*) (Palmer, *et al.*, 1996) cells were used for the co-expression of mAOX3 wild-type with mMCSF (pSS110) (Schumann, *et al.*, 2009). *E.coli* expression cultures were grown in LB medium, under aerobic conditions at 30°C for 24h.

Cloning and Expression

The cDNA of mAOX3 was cloned from mouse CD1 liver (Vila, *et al.*, 2004), using primers designed to permit cloning into the *NdeI* and *SalI* sites of the expression vector pTrcHis (Temple & Rajagopalan, 2000). The resulting plasmid was designated pMMA1 which expresses mAOX3 as a N-terminal fusion protein with a His_6-tag. For heterologous expression in *E. coli*, pMMA1 and pSS110 (Schumann, *et al.*, 2009) were transformed into TP1000 cells. To express the recombinant proteins, cells were grown at 30°C in 14 L LB medium supplemented with 150 µg/mL ampicillin, 50 µg/ml chloramphenicol, 1 mM molybdate, and 10 µM IPTG.

Purification of recombinant mAOX3

After 24h expression at 30°C and low aeration, the cells were harvested by centrifugation and resuspended in 50 mM sodium phosphate buffer pH 8.0, 300 mM NaCl. To disrupt the cells, a cell disruptor was used (Constant Cell Systems TS Benchtop Series) at 12°C and 1.35 kbar, in the presence of DNaseI and Lysozyme (1 mg/L). The cleared lysate was loaded onto a Ni^{2+}-nitriloacetic (Ni-NTA, Qiagen) column using 0.2 ml of resin per culture Liter. Two washing steps were performed with 35 mM and 50 mM imidazole, and mAOX3 was eluted with 250 mM imidazole.

DMD Fast Forward. Published on June 24, 2011 as DOI: 10.1124/dmd.111.040873
This article has not been copyedited and formatted. The final version may differ from this version.

Buffer was exchanged to 50 mM potassium phosphate, pH 7.8, 0.1 mM EDTA, using PD10 columns (GE Healthcare). To increase the activity of the enzyme, chemical sulfuration was performed under conditions similar to those reported previously (Massey & Edmondson, 1970, Wahl, *et al.*, 1982). The purified enzyme was incubated for 1h with 500 µM sodium dithionite, 25 µM methylviologen and 2 mM sodium sulfide in an anaerobic chamber (Coy Lab Systems). After buffer exchange to 50 mM sodium phosphate pH 8.0, 300 mM NaCl, the protein sample was loaded onto a Superose 6 column (GE Healthcare), and fractions containing dimeric mAOX3 were combined and stored in 100 mM potassium phosphate pH 7.4, at -80°C.

To cleave the N-terminal His_6-tag, the enzyme was incubated in 50 mM Tris-HCl, pH 8.0, 1 mM EDTA at 4°C for 12 h. The thrombin cleavage site introduced by pTrc-His was used, and the 17 amino acid sequence containing His_6-tag was cleaved after Arg17 (Temple & Rajagopalan, 2000). The protein was purified afterwards by size exclusion chromatography using a HiLoad 26/60 Superdex 200 column (GE Healthcare), equilibrated with 50 mM sodium phosphate pH 8.0, 300 mM NaCl. The fractions containing the dimeric ΔHis_6-mAOX3 were combined and concentrated by ultrafiltration (Amicon 50 kDa MWCO, Millipore, USA), to a final concentration of 17.8 mg/ml. Protein aliquots were frozen in liquid nitrogen and stored at -80°C until usage, without loss of activity.

Purification of native mAOX3

Native mAOX3 was purified following the protocol described by Terao et al. (Terao, *et al.*, 2001). 100 CD1 mouse livers were homogenized in three volumes of sodium phosphate buffer pH 7.5 with an ultraturrax (Omni 2000, Omni International, Waterbury, CT), and the cleared lysate was heated to 55°C for 10 minutes. After

DMD Fast Forward. Published on June 24, 2011 as DOI: 10.1124/dmd.111.040873
This article has not been copyedited and formatted. The final version may differ from this version.

ammonium sulfate precipitation overnight (50% saturation), the pellet was solved and subjected to benzamidine sepharose chromatography. The protein was further purified using a linear NaCl gradient on a 5/5 FPLC Mono Q column (Amersham).

SDS-polyacrylamide Gel Electrophoresis (PAGE)

SDS-PAGE was performed as described by Laemmli using 10% polyacrylamide gels. The gels were stained with Coomassie Brilliant Blue R. The mAOX3 activity was visualized on native polyacrylamide gels by staining with 25 mM benzaldehyde and 1 mM MTT in 50 mM Tris, pH 8.0 (Perez-Vicente, *et al.*, 1992).

Enzyme assays

Enzyme assays were performed at 37°C in 50 mM Tris-HCl pH 8.0, 1 mM EDTA, with variable substrate (0-250 µM benzaldehyde, 0-10 mM butyraldehyde, 0-500 µM 2-OH-pyrimidine), and purified mAOX3 (50-200 nM) concentrations. As electron acceptors, 100 µM DCPIP or 1 mM potassium ferricyanide were used in a final reaction volume of 500 µL. Enzyme activity was monitored at 600 nm for DCPIP and at 420 nm for ferricyanide. Specific activity was calculated using the molecular extinction coefficient of 21,400 $M^{-1}cm^{-1}$ for mAOX3. Kinetic parameters were obtained by nonlinear fitting of the Michaelis-Menten equation or the substrate inhibition equation using R build 2.12.00 (Team, 2010).

Metal analysis by ICP-MS

The molybdenum and iron contents were determined using induced coupled plasma mass spectrometry (ICP-MS, PerkinElmer PE SCIEX ELAN6000). Samples of 500 µl containing 5 µM of protein were wet-ashed with 32.5% nitric acid at 100°C

overnight. 300 µL of the wet-ashed sample were diluted with H_2O into 5 mL, and metal presence was quantified by ICP-MS using a multielement standard solution (XVI, Merck Germany) and an internal Yttrium standard.

FAD analysis by HPLC

FAD was determined by the AMP content after hydrolysis of 20 µM mAOX3 in 5% sulfuric acid for 10 minutes at 95°C. Released AMP was detected on a C18 reversed phase column as reported previously (Schmitz, *et al.*, 2008) and quantified against a FAD standard.

CD-spectroscopy

UV/visible CD spectra of 8 µM enzyme samples were recorded in 50 mM potassium phosphate, and 0.1 mM EDTA at pH 7.8, using a Jasco J-715 CD-spectrophotometer. The scanning mode was set step-wise, and for each nm a data pitch was recorded with response time of 2 seconds, and each measurement was repeated 4 times.

Electron Paramagnetic Resonance Spectroscopy

9.5 GHz X-band EPR spectra were recorded on a Bruker ESP300E spectrometer equipped with a TE_{102} microwave cavity. For temperature control between 5 K und 300 K an Oxford ESR 900 helium flow cryostat with an Oxford ITC4 temperature controller was used. The microwave frequency was detected with an EIP frequency counter (Microwave Inc.). Magnetic field was calibrated using a Li/LiF standard with a known g-value of 2.002293 ± 0.000002 (Stesmans & Vangorp, 1989). Samples (typically 0.1 mM enzyme) were prepared in quartz tubes with 4 mm outer diameter. Chemical reduction to generate the reduced Fe(II)/Fe(III) form of the FeS clusters,

was performed by adding a small volume of anaerobic sodium dithionite solution to the protein solution under a weak stream of argon gas (20-fold excess dithionite with respect to the protein). The sample tubes were frozen, after a change of colour was observed (typically 30 s reaction time) in liquid nitrogen. Baseline corrections, if required, were performed by subtracting a background spectrum, obtained under the same experimental conditions from a sample containing only a buffer solution. Simulations of the experimental EPR spectra, based on a spin Hamilton operator approach, were performed with the program *EasySpin* (Stoll & Schweiger, 2006).

Crystallization

Initial crystallization studies were pursued with the purified recombinant mAOX3. Several additives as well as some known mAOX3 inhibitors (e.g. menadione) were tested to optimize the crystals. Ionic liquids ($[C_4mim]Cl^-$ and $[C_4mim]MDEGSO_4$) were also tested as additives since, in a similar case of crystal optimization, this proved to be a very attractive alternative (Coelho, *et al.*, 2010). The best protein needles of recombinant mAOX3 were obtained in the following conditions: 12-16% PEG 8000, 0.1 M potassium phosphate pH 7.0, equal amounts of protein (17.8 mg/ml, incubated with fresh DTT at 4ºC for 1h) and precipitant solutions, at 20ºC (Fig.1A). Since His-tags usually have little effect on the protein native structure, but can have an impact in crystallization (Carson, *et al.*, 2007) the recombinant protein His_6-tag (with 17 residues) was cleaved. With this protein preparation, crystals were also formed under similar conditions but without significant improvement.

Similar crystallization conditions were tested mouse liver mAOX3: buffer pH was adjusted to 6.5; protein concentration was decreased to 10 mg/ml; and 2 mM EDTA was added to the crystallization solution. Larger, rectangular-shaped crystals (0.40 x

0.15 x 0.05 mm, Fig.1B) of the native mAOX3 were reproducibly formed. These were the only crystals that allowed collecting a usable diffraction data set.

Data Collection, Processing and Structure Solution

All tested crystals were flash-cooled directly in liquid nitrogen, using paratone oil as cryoprotectant. Some of the native mAOX3 crystals diffracted to ~6 Å but after annealing, diffraction improved dramatically, to a resolution beyond 3 Å (Figure 2). A first data set (mNAT-I) consisting of 180º of data was collected at ID14-1 in the European Synchrotron Radiation Facility (ESRF, Grenoble, France) (Table 1). The crystal belong to space group P1, with unit cell dimensions a = 91.07 Å, b = 135.02 Å, c = 147.48 Å, α = 78.27º, β = 77.77º and γ = 89.96º. The calculated Matthews coefficient was 2.89 $Å^3Da^{-1}$, corresponding to two dimers in the unit cell with a solvent content of 57.4% (Matthews, 1968). Because the data were very anisotropic and the mosaicity was high, the initial data processing using imosflm 1.0.4 was incomplete (~89% complete to 2.9 Å) (Leslie, 1992). The same crystal was later measured at ID23-1 at the ESRF. Although a full 360º of data were collected, only about 220º were useable (mNAT-II) because the crystal was very anisotropic. The two data sets were merged together to increase the completeness and improve the multiplicity. The resulting dataset presents very high Rpim (as expected) and is only ~80% complete to 2.9 Å (mNAT), but the overall redundancy improved to ~3.0. The structure of the mAOX3 will be solved by molecular replacement using BALBES on the mNAT-I data set (Long, *et al.*, 2008) in the future. The bovine milk XDH structure (PDB code 3BDJ) can be used as a search model (Okamoto, *et al.*, 2008) and four monomers were found in the unit cell.

DMD Fast Forward. Published on June 24, 2011 as DOI: 10.1124/dmd.111.040873
This article has not been copyedited and formatted. The final version may differ from this version.

Results and Discussion

Comparison of recombinant mAOX3 expressed in *E. coli* with the native protein purified from mouse livers.

Several heterologous expression systems for mammalian AO have been described. So far, a main drawback of these systems is the low catalytic activity of the purified enzymes due to the low Moco content or reduced content of the terminal Mo=S ligand at the Mo site (Huang, *et al.*, 1999, Adachi, *et al.*, 2007). In a previous report, we described a successful purification of mouse AOX1 (mAOX1) in an active form, after simultaneous expression of mAOX1 and the mouse Moco sulfurase (mMCSF) in *E. coli* TP1000 cells (Schumann, *et al.*, 2009). This approach ensured a higher level of sulfurated Moco insertion into the enzyme and resulted in a 20% active enzyme which could be purified in a reproducible manner. We adapted this system for the expression of mAOX3. Comparison of the activity of mAOX3 after expression in the presence or absence of mMCSF showed that the content of the terminal sulfur ligand was 19% increased in the presence of mMCSF (data not shown). Thus, we have used this system for the expression of catalytically active recombinant mAOX3.

Recombinant mAOX3 was purified from a 14 L *E. coli* culture using sequential Ni-NTA chromatography and size exclusion chromatography. In addition, a chemical sulfuration step was performed to further increase the activity of the enzyme 1.4-fold (Table 2). The purification protocol used for mAOX3 is summarized in Table 2. The overall purification of recombinant mAOX3 from the soluble fraction was more than 35.7 fold with a yield of 2.3%. The total yield was 0.8 mg pure enzyme per liter of *E. coli* culture. For comparison, we also purified native mAOX3 from CD1 livers according to the protocol described in (Terao, *et al.*, 2001).

SDS polyacrylamide gels performed under reducing conditions demonstrated the

presence of one major band with a size of 150 kDa for both proteins after purification (Fig. 3). Under these experimental conditions, additional bands of minor intensity with sizes of 130, 80, 70, and 55 kDa were observed for the recombinant protein, which were not present in the native mAOX3 (Fig. 3). Electrospray mass spectrometry analysis revealed that these bands were degradation products of mAOX3 (data not shown). These degradation products were only detected after incubation of the protein with β-mercaptoethanol. Both proteins were detectable as a single band in native PAGE visualized by activity staining or Coomassie blue staining (Fig. 4). The recombinant protein has a slightly different migration behavior on polyacrylamide gels due to the presence of the N-terminal His_6-tag (~ 2 kDa). Both native and recombinant mAOX3 eluted from size exclusion chromatography mainly at a size of ~300 kDa indicating a functional dimer as the main product of expression and purification (data not shown). The UV-vis spectra of both proteins are identical and display the typical features of MFE's (Fig. 5). The A280/A444 ratio of 5.2 for the recombinant protein indicates a high purity of the enzyme. The proportion for the native enzyme was similar. The 444/550 absorbance ratio in the UV-vis spectrum was calculated to be 3.1 for the recombinant enzyme and 3.1 for the native enzyme, demonstrating that both proteins were fully saturated with FAD. Additionally, the FAD content of both proteins was determined to be 100% by quantifying the AMP content of the protein. The molybdenum and iron content were quantified by inductively coupled plasma-optical emission spectroscopy (ICP-MS, Table 3) and revealed a level for the recombinant mAOX3 of 58.0 ± 0.2% saturation for molybdenum and 57.6 ± 0.3% saturation for iron (with respect to the 2x[2Fe-2S] clusters). For the native mAOX3, the molybdenum saturation was determined to be 103.8 ± 0.2% and the iron saturation to be 53.0 ± 0.6%. Thus, the overall metal

content for both proteins is comparable, but displays an incomplete saturation for both metals. The cyanolyzable sulfur was determined to be present to 33 ± 0.5% for recombinant mAOX3, while the native protein is expected to be fully sulfurated when the activities of the two enzymes are compared (see below).

Steady state kinetics of mAOX3 with different substrates.

Apparent k_{cat} and K_M values where determined by rate of $K_3[Fe(CN)_6]$ reduction at 420 nm and 25°C in 100 mM potassium phosphate buffer pH 7.4 (Table 4). Initial rates were plotted against substrate concentrations and fitted nonlinearly to the Michaelis-Menten equation. As substrates, benzaldehyde, 2-OH-pyrimidine and butanal were used and the results were found to be similar to literature data (Vila, *et al.*, 2004). Kinetic parameters of native and recombinant mAOX3 are in agreement considering that the activity of the recombinant enzyme is only 30% due to the limited saturation of the cyanolyzable sulfur ligand. The values reported in the literature are slightly different, probably due to different experimental conditions.

CD spectroscopy

CD spectra of the air-oxidized forms were measured in region from 250 to 850 nm. The spectra of the recombinant and native mAOX3 were found to be identical (Fig.6). The spectra of the oxidized enzymes exhibited strong negative dichroic bands at approximately 350 - 400 nm and 520 - 580 nm, and intensive positive bands between 400 and 500 nm (Fig.6). From the various maxima and inflections, transitions can be identified at 380 (-), 432 (+), 474 (+), and 552 (-) nm. The visible CD spectra of oxidized mAOX3 for the recombinant and the native protein are similar. There are differences in comparison to the CD spectrum obtained for mAOX1 (Schumann, *et*

al., 2009), especially in the region around 372 and 434 nm, indicating differences in the structure of FeSII.

EPR spectroscopy of the mAOX3 [2Fe-2S] clusters.

Since the purified mAOX3 proteins showed a reduced level of iron, the [2Fe-2S] clusters were characterized by EPR spectroscopy. Fig. 7 shows the EPR spectra of native and recombinant dithionite-reduced mAOX3 wild-type together with the corresponding simulations. The spectra display signals from several superimposed paramagnetic species, which are usually observed for enzymes of the XO family. However, the most prominent signals are the characteristic EPR signals assigned to the two iron sulfur centers FeSI and FeSII, which are similar for all members of the XO family that have been described to date (Hille, 1996, Parschat, *et al.*, 2001). FeSI has EPR properties showing a rhombic g-tensor, similar to those of many other [2Fe-2S] proteins, being fully developed at relatively high temperatures (up to T = 80 K), while FeSII has unusual EPR properties for [2Fe-2S] species with a strongly rhombic g-tensor, showing broad lines that can only clearly be observed at much lower temperatures (T < 40 K). The g-values and line widths were evaluated by simulating the spectra using the program *EasySpin* (Stoll & Schweiger, 2006). In both proteins, FeSI has similar EPR properties, including the typical, rhombic g-tensor as observed for other [2Fe2S] of the ferredoxin-type (see Table 5). The spectra indicate heterogeneities of FeSI, which can be seen especially for the g_x-components. FeSII shows only weak signals in both mAOX3 preparations at lower temperatures indicating an incomplete saturation of FeSII for both the recombinant and native mAOX3. Native mAOX3, however, displays a slightly higher amount of FeSII. Under the experimental conditions to reduce the proteins, no clear signals of the reduced

DMD Fast Forward. Published on June 24, 2011 as DOI: 10.1124/dmd.111.040873
This article has not been copyedited and formatted. The final version may differ from this version.

flavin semiquinone (FAD) or Moco (Mo^{V}) were observed. The line widths and positions of the FeS signals at lower temperatures were affected by magnetic interactions. Due to the additional heterogeneities present in the samples, a reliable simulation of FeSII to determine the exact level of FeSII saturation in the enzymes was not possible. We, therefore, report only the g-values for FeSI. The obtained g-tensor and line width for FeSI of mAOX3 are almost identical to the values previously published for mAOX1 (Schumann, *et al.*, 2009) indicating the high structural similarity of the proteins as expected from the amino acid sequence identity of 61%.

Protein crystallization, data collection and structure solution

Expression and purification of the recombinant mAOX3 was crucial for the crystallization and structure determination of the native protein. The vast majority of the crystallization trials were performed using the recombinant protein (Fig. 1A), overcoming the restrictions imposed by the limited amount of the native mouse protein available. Thus, it was possible to identify suitable crystallization conditions, which were successfully applied to the native protein purified from the mouse liver (Fig. 1B). In spite of the very difficult handling of the crystals and the fact that most of the crystals tested for diffraction did not yield measurable data, we were able to obtain a usable data set with 2.9 Å resolution at ID14-1 and ID23-1 at the ESRF (Figure 2). With these data, the structure of mAOX3 can be solved by molecular replacement methods in the future, using the homologous XOR as a search model. The present work constitutes a major achievement since it will help to obtain the first crystal structure of AO, an enzyme of well-known importance in drug metabolism, and therefore of increasing importance in recent drug design programs (Pryde, *et al.*,

2010). Besides, the crystal structure of mAOX3 will allow explaining and understanding the mechanistic and substrate specificity differences observed between AO and XOR, despite their remarkable similarity.

Conclusions

We have reported a system for the heterologous expression of mAOX3 in *E. coli*. To ensure a higher sulfuration level of mAOX3, we engineered *E.coli* for the simultaneous expression of the mMCSF and mAOX3 proteins, as reported before for mAOX1 (Schumann, *et al.,* 2009). After coexpression with mMCSF and chemical sulfuration, 30% of mAOX3 exist in the catalytically active form. The recombinant mAOX3 displays similar catalytic properties in comparison to the enzyme purified from mouse livers. This finding demonstrates that the protein was correctly folded in mMCSF engineered *E. coli* cells and could be used for more detailed analyses. The recombinant enzyme displayed only 30% of the activity with benzaldehyde, butyraldehyde, or 2-OH-pyrimidine as substrates in comparison to the native enzyme, values which are consistent with its sulfuration level. Both the recombinant and the native mAOX3 were compared in detail on the basis of their spectroscopic properties. The EPR spectra of mAOX3 were found to be very similar to those from the mAOX1 protein, showing a rhombic signal for FeSI (Schumann, *et al.*, 2008). There are essentially no differences in the g-values and line widths for the native and the recombinant enzyme. However, in particular the FeSII center was not fully saturated in both enzymes, a finding that is consistent with the iron saturation of both enzymes. Since FeSII is the more surface exposed FeS cluster of the two, as revealed by the crystal structure of bovine XO/XDH, it might be possible that the cluster is partially lost during the purification of the enzymes. At least, the lower saturation of FeSII is

not based on the inability of the *E. coli* system to insert the cluster correctly, since both enzymes display almost identical EPR spectra. Overall, the close similarity of the EPR parameters indicated the presence of the same ligands and similar geometries of the two redox centers in comparison to mAOX1. The recombinant enzyme was used to optimize the crystallization conditions for the native enzyme. We were able to obtain a usable data set at 2.9 Å resolution with crystals of native mAOX3. This is a major achievement for the characterization of AO, an enzyme of well-known importance in drug metabolism, and therefore of increasing importance in recent drug design programs

In total, the established expression system of mAOX3 in *E. coli* can further be used for detailed site-directed mutagenesis and structure-function studies of this enzyme.

Acknowledgements:

We thank Manfred Nimtz (Braunschweig) for MALDI peptide mapping and the ID 14-1 ID23-2 staff of ESRF (Grenoble, France), for assistance during data collection.

Authorship Contributions.

Participated in research design: Mahro, Coelho, Trincao, Rodriguez, Lendzian, Garattini, Romao, Leimkühler

Conducted experiments: Mahro, Coelho, Trincao, Rodriguez, Saggu, Terrao

Contributed new reagents or analytic tools: Coelho,

Performed data analysis: Mahro, Coelho, Trincao, Saggu, Lendzian, Leimkühler

Wrote or contributed to the writing of the manuscript: Mahro, Coelho, Trincao, Saggu, Lendzian, Terrao, Garattini, Hildebrandt, Romao, Leimkühler

References

Adachi M, Itoh K, Masubuchi A, Watanabe N & Tanaka Y (2007) Construction and expression of mutant cDNAs responsible for genetic polymorphism in aldehyde oxidase in Donryu strain rats. *J Biochem Mol Biol* **40**: 1021-1027.

Carson M, Johnson DH, McDonald H, Brouillette C & Delucas LJ (2007) His-tag impact on structure. *Acta crystallographica. Section D, Biological crystallography* **63**: 295-301.

Coelho C, Trincao J & Romao MJ (2010) THe use of ionic liquids as crystallization additives alowed to overcome nanodrop scaling up problems: A sucess case for producing diffraction-quality crystals of nitrate reductase. *Journal of Crystal Growth* **312**: 714-719.

Garattini E & Terao M (2011) Increasing recognition of the importance of aldehyde oxidase in drug development and discovery. *Drug Metab Rev*. in press.

Garattini E, Fratelli M & Terao M (2008) Mammalian aldehyde oxidases: genetics, evolution and biochemistry. *Cell Mol Life Sci* **65**: 1019-1048.

Garattini E, Mendel R, Romao MJ, Wright R & Terao M (2003) Mammalian molybdo-flavoenzymes, an expanding family of proteins: structure, genetics, regulation, function and pathophysiology. *Biochem J* **372**: 15-32.

Hille R (1996) The mononuclear molybdenum enzymes. *Chemical Rev* **96**: 2757-2816.

Huang DY, Furukawa A & Ichikawa Y (1999) Molecular cloning of retinal oxidase/aldehyde oxidase cDNAs from rabbit and mouse livers and functional expression of recombinant mouse retinal oxidase cDNA in Escherichia coli. *Arch Biochem Biophys* **364**: 264-272.

Krenitsky TA (1978) Aldehyde oxidase and xanthine oxidase—functional and evolutionary relationships. *Biochem. Pharmacol.* **27**: 2763-2764.

Krenitsky TA, Neil SM, Elion GB & Hitchings GH (1972) A comparison of the specificities of xanthine oxidase and aldehyde oxidase. *Arch. Biochem. Biophys.* **150**: 585-599.

Leslie AGW (1992) Recent changes to the MOSFLM package for processing film and image plate data. *Joint CCP4 * ESF-EAMCB Newsletter on Protein Crystallography* **26**.

Long F, Vagin AA, Young P & Murshudov GN (2008) BALBES: a molecular-replacement pipeline. *Acta crystallographica. Section D, Biological crystallography* **64**: 125-132.

Massey V & Edmondson D (1970) On the mechanism of inactivation of xanthine oxidase by cyanide. *J. Biol. Chem.* **245**: 6595-6598.

Matthews BW (1968) Solvent content of protein crystals. *Journal of molecular biology* **33**: 491-497.

Nishino T, Okamoto K, Eger BT & Pai EF (2008) Mammalian xanthine oxidoreductase - mechanism of transition from xanthine dehydrogenase to xanthine oxidase. *The FEBS journal* **275**: 3278-3289.

Okamoto K, Eger BT, Nishino T & Pai EF (2008) Mechanism of inhibition of xanthine oxidoreductase by allopurinol: crystal structure of reduced bovine milk xanthine oxidoreductase bound with oxipurinol. *Nucleosides, nucleotides & nucleic acids* **27**: 888-893.

Palmer T, Santini C-L, Iobbi-Nivol C, Eaves DJ, Boxer DH & Giordano G (1996) Involvement of the *narJ* and *mob* gene products in the biosynthesis of the

molybdoenzyme nitrate reductase in *Escherichia coli*. *Mol Microbiol* **20**: 875-884.

Parschat K, Canne C, Huttermann J, Kappl R & Fetzner S (2001) Xanthine dehydrogenase from Pseudomonas putida 86: specificity, oxidation-reduction potentials of its redox-active centers, and first EPR characterization. *Biochim Biophys Acta* **1544**: 151-165.

Perez-Vicente R, Alamillo JM, Cardenas J & Pineda M (1992) Purification and substrate inactivation of xanthine dehydrogenase from Chlamydomonas reinhardtii. *Biochimica et biophysica acta* **1117**: 159-166.

Pryde DC, Dalvie D, Hu Q, Jones P, Obach RS & Tran TD (2010) Aldehyde oxidase: an enzyme of emerging importance in drug discovery. *Journal of medicinal chemistry* **53**: 8441-8460.

Schmitz J, Chowdhury MM, Hanzelmann P, Nimtz M, Lee EY, Schindelin H & Leimkuhler S (2008) The sulfurtransferase activity of Uba4 presents a link between ubiquitin-like protein conjugation and activation of sulfur carrier proteins. *Biochemistry* **47**: 6479-6489.

Schumann S, Saggu M, Möller N, Anker SD, Lendzian F, Hildebrandt P & Leimkühler S (2008) The mechanism of assembly and cofactor insertion into *Rhodobacter capsulatus* xanthine dehydrogenase. *J Biol Chem* **283**: 16602-16611.

Schumann S, Terao M, Garattini E, Saggu M, Lendzian F, Hildebrandt P & Leimkuhler S (2009) Site directed mutagenesis of amino acid residues at the active site of mouse aldehyde oxidase AOX1. *PloS one* **4**: e5348.

Stesmans A & Vangorp G (1989) Novel Method for Accurate G-Measurements in Electron-Spin Resonance. *Journal of Magnetic Resonance* **178**: 42-55.

Stoll S & Schweiger A (2006) EasySpin, a comprehensive software package for spectral simulation and analysis in EPR. . *J Magn Reson* **178**: 42-55.

Team RDC (2010) *R: A Language and Environment for Statistical Computing.*

Temple CA & Rajagopalan KV (2000) Optimization of Expression of Human Sulfite Oxidase and its Molybdenum Domain. *Arch. Biochem. Biophys.* **383**: 281-287.

Terao M, Kurosaki M, Barzago MM, *et al.* (2006) Avian and canine aldehyde oxidases. Novel insights into the biology and evolution of molybdo-flavoenzymes. *The Journal of biological chemistry* **281**: 19748-19761.

Terao M, Kurosaki M, Marini M, *et al.* (2001) Purification of the aldehyde oxidase homolog 1 (AOH1) protein and cloning of the AOH1 and aldehyde oxidase homolog 2 (AOH2) genes. Identification of a novel molybdo-flavoprotein gene cluster on mouse chromosome 1. *J Biol Chem* **276**: 46347-46363.

Vila R, Kurosaki M, Barzago MM, *et al.* (2004) Regulation and biochemistry of mouse molybdo-flavoenzymes. The DBA/2 mouse is selectively deficient in the expression of aldehyde oxidase homologues 1 and 2 and represents a unique source for the purification and characterization of aldehyde oxidase. *J Biol Chem* **279**: 8668-8683.

Wahl RC & Rajagopalan KV (1982) Evidence for the inorganic nature of the cyanolyzable sulfur of molybdenum hydroxylases. *J. Biol. Chem.* **257**: 1354-1359.

Wahl RC, Warner CK, Finnerty V & Rajagopalan KV (1982) *Drosophila melanogaster ma-l* mutants are defective in the sulfuration of desulfo Mo hydroxylases. *J. Biol. Chem.* **257**: 3958-3962.

Footnotes:

(*) These authors contributed equally to this work.

This work was supported by the Cluster of Excellence 'Unifying Concepts in Catalysis' coordinated by the Technische Universität Berlin. Grant [SFRH/BD/37948/2007 (CC)] and project [PTDC/QUI/64733/2006] were financed by the Fundação para a Ciência e Tecnologia, Portugal. The exchange of researchers among laboratories involved in the work was funded by the DAAD-GRICES program.

DMD Fast Forward. Published on June 24, 2011 as DOI: 10.1124/dmd.111.040873
This article has not been copyedited and formatted. The final version may differ from this version.

FIGURE LEGENDS:

Figure 1 – Crystals of mAOX3 protein: (a) needles from the recombinant protein, and (b) crystals from native mouse liver protein

Figure 2 – Diffraction pattern of the native mouse liver AOX3 protein obtained at ID14-1 (A) before (upper left quadrant) and after re-annealing; and obtained at ID23-1 (ESRF) (B). The resolution at the edge is 3.0 Å in both images.

Figure 3 - Purification of mAOX3 after heterologous expression in *E. coli*. 12% SDS-PAGE analysis of mAOX3 purification. The protein was purified after Ni-NTA, a chemical sulfuration step, and Superose 6 chromatography. Purified mAOX1 displays a molecular mass of 150 kDa on SDS-PAGE, the bands with sizes of 130 kDa, 80 kDa, 70 kDa, and 50 kDa correspond to degradation products of recombinant mAOX3, as determined by mass spectrometry. (1) Recombinant mAOX3 *E. coli* crude extract; (2) recombinant mAOX3 after Ni-NTA chromatography; (3) recombinant mAOX3 after chemical sulfuration; (4) recombinant mAOX3 after Superose 6 chromatography; (5) native mAOX3.

Figure 4 - Comparison of recombinant and native mAOX3 by SDS-PAGE and native PAGE. (A) Purified mAOX3 (2 µg per lane) was analyzed by 10% SDS-PAGE and stained by Coomassie blue. Bands at molecular weight of 130 kDa, 80kDa, 70 kDa and 50 kDa were identified as degradation products by ESI-MS analysis: 1, recombinant mAOX3; 2, native mAOX3. (B) Native PAGE of purified mAOX3 (2 µg per lane) was stained by activity staining with 25 mM benzaldehyde and 1 mM MTT as substrates: 3,

recombinant mAOX3; 4, native mAOX3. Recombinant mAOX3 has reduced gel mobility due to the N-terminal His_6-tag which increases the molecular mass about 2 kDa.

Figure 5 - Characterization of native and recombinant mAOX3 by UV-VIS absorption spectroscopy. Spectra of air-oxidized recombinant mAOX3 (solid line) and native mAOX3 (dotted line) were recorded in 50 mM potassium phosphate pH 7.4 under aerobic conditions. Recorded spectra were normalized to a concentration of 10 µM.

Figure 6 – CD-spectra of native and recombinant mAOX3. Spectra recombinant mAOX3 (solid line) and native mAOX3 (dotted line) were recorded in 50 mM potassium phosphate, 0.1 mM EDTA, pH 7.8 at 10°C using a Jasco J-715 CD-spectrometer. The protein concentration was 8 µM.

Figure 7 - EPR spectra of native and recombinant mAOX3. The figure shows the dithionite reduced native mAOX3 (upper spectrum) and recombinant mAOX3 (lower spectrum) at temperatures of 40 K and 10 K together with the corresponding simulations (dashed traces). In both proteins FeSI has similar EPR properties, showing a rhombic g-tensor as observed for other [2Fe-2S] ferredoxins. FeSII shows only weak signals in mAOX3 at 10 K, whereas a slightly higher amount of FeSII is observed in native mAOX3.

DMD Fast Forward. Published on June 24, 2011 as DOI: 10.1124/dmd.111.040873
This article has not been copyedited and formatted. The final version may differ from this version.

Table 1. X-ray crystallography data-collection statistics.

Crystal Sample	mNAT-I	mNAT-II	mNAT (merged)[a]
X-ray source	ID 14-1	ID 23-2	-
Crystal system	Triclinic		
Unit-cell parameters (Å, º)	*a* = 91.07, *b* = 135.02, *c* = 147.48 α = 78.27, β = 77.77, γ = 89.96	*a* = 91.54, *b* = 135.83, *c* = 147.84 α = 78.22, β = 77.89, γ = 89.97	-
Maximum resolution (Å)	2.9	3.2	3.0
Mosaicity (º)	1.0	1.0	1.0
Molecules per ASU	4		
Matthews coefficient ($Å^3$/Da)	2.89	2.93	-
Space group	P1		
Wavelength (Å)	0.934	0.975	-
No. observed reflections	219268 (20892)	223954 (24999)	338761 (41810)
No. unique reflections	133319 (16784)	78529 (10857)	112209 (16428)
Resolution limits (Å)	51.1 – 2.9	50.0 – 3.2	50 .0 – 3.20
Redundancy	1.6 (1.2)	2.8 (2.2)	3.0 (2.5)
Completeness (%)	89.8 (77.3)	69.5 (65.1)	81.8 (81.7)
R_{pim} (%)	5.6 (14.0)	14.3 (68.9)	17.5 (63.4)
I / σ	9.6 (3.6)	6.3 (1.4)	7.0 (4.2)

[a] Values in parenthesis correspond to the highest resolution shell

DMD Fast Forward. Published on June 24, 2011 as DOI: 10.1124/dmd.111.040873
This article has not been copyedited and formatted. The final version may differ from this version.

Table 2. Purification of recombinant mAOX3 after expression in *E. coli* TP1000 cells.

			Benzaldehyde:DCPIP activity [b)]			
Step	**Volume**	**Total protein [a)]**	**Total actvity [c)]**	**S.A.**	**Yield**	**-fold**
	mL	mg	IU	IU/mg	%	purification
Crude Extract	280	17513	163.3	0.009	77	0.8
Cleared Lysate	280	18354	212.9	0.012	100	1.0
Flow Trough	280	18597	170.8	0.009	80	0.8
Ni-NTA	30.4	35	3.6	0.104	1.71	9.0
Chemical Sulfuration	49.4	32	5.0	0.158	2.34	13.6
Superose 6	15.2	12	4.9	0.414	2.30	35.7

[a] Total protein was quantified with the Bradford assay.

[b] The activity was measured by monitoring the decrease in absorption at 600 nm in the presence of 250 µM benzaldehyde and 100 µM DCPIP.

[c] S.A.: Specific enzyme activity (units/mg) is defined as the oxidation of 1 µM benzaldehyde per min and mg of enzyme under the assay conditions.

DMD Fast Forward. Published on June 24, 2011 as DOI: 10.1124/dmd.111.040873
This article has not been copyedited and formatted. The final version may differ from this version.

Table 3. Determination of the molybdenum and iron content for native and recombinant mAOX3.

mAOX3	% Mo content[a]	% Fe-content[b]
native	103 ± 0.2	53 ± 0.6
recombinant	58 ± 0.2	57 ± 0.3

[a] Molybdenum was quantified as described by ICP-MS, in Materials and Methods.

[b] Iron was determined by ICP-MS, as described in Materials and Methods.

DMD Fast Forward. Published on June 24, 2011 as DOI: 10.1124/dmd.111.040873
This article has not been copyedited and formatted. The final version may differ from this version.

Table 4. Steady-state kinetic parameters of recombinant and native mAOX3, with different aldehyde and purine substrates.

	native mAOX3				recombinant mAOX3			
	k_{cat}[a]		K_M[a]		k_{cat}[a]		K_M[a]	
	1/min		µM		1/min		µM	
benzaldehyde	130 ± 8		13 ± 6		44 ± 2		20 ± 6	
butyraldehyde	384 ± 40		29 ± 8		140 ± 10		26 ± 5	
2-OH-pyrimidine	1279 ± 55		173 ± 18		413 ± 16		97 ± 11	

[a]Apparent kinetic parameters were recorded in 100 mM potassium phosphate, pH 7.4 by varying the concentration of substrate in the presence of 1 mM ferricyanide as electron acceptor.

DMD Fast Forward. Published on June 24, 2011 as DOI: 10.1124/dmd.111.040873
This article has not been copyedited and formatted. The final version may differ from this version.

Table 5. EPR linewidths and g-values of FeSI and FeSII from mAOX3.

Sample	Cluster	g-value				linewidth [mT]
		g_x [a]	g_y	g_z [b]	g_{av}	
native mAOX3	FeSI (40K)	2.023 (0.005)	1.932	1.904 (0.015)	1.95	1.9
recombinant mAOX3	FeSI (40K)	2.023 (0.005)	1.932	1.904 (0.015)	1.95	1.9

[a] g-strain was included in the simulation with 0.04 for g_x. Numbers in brackets are **e**stimated error of g-values

[b] g-strain was included in the simulation with 0.01 for g_z.

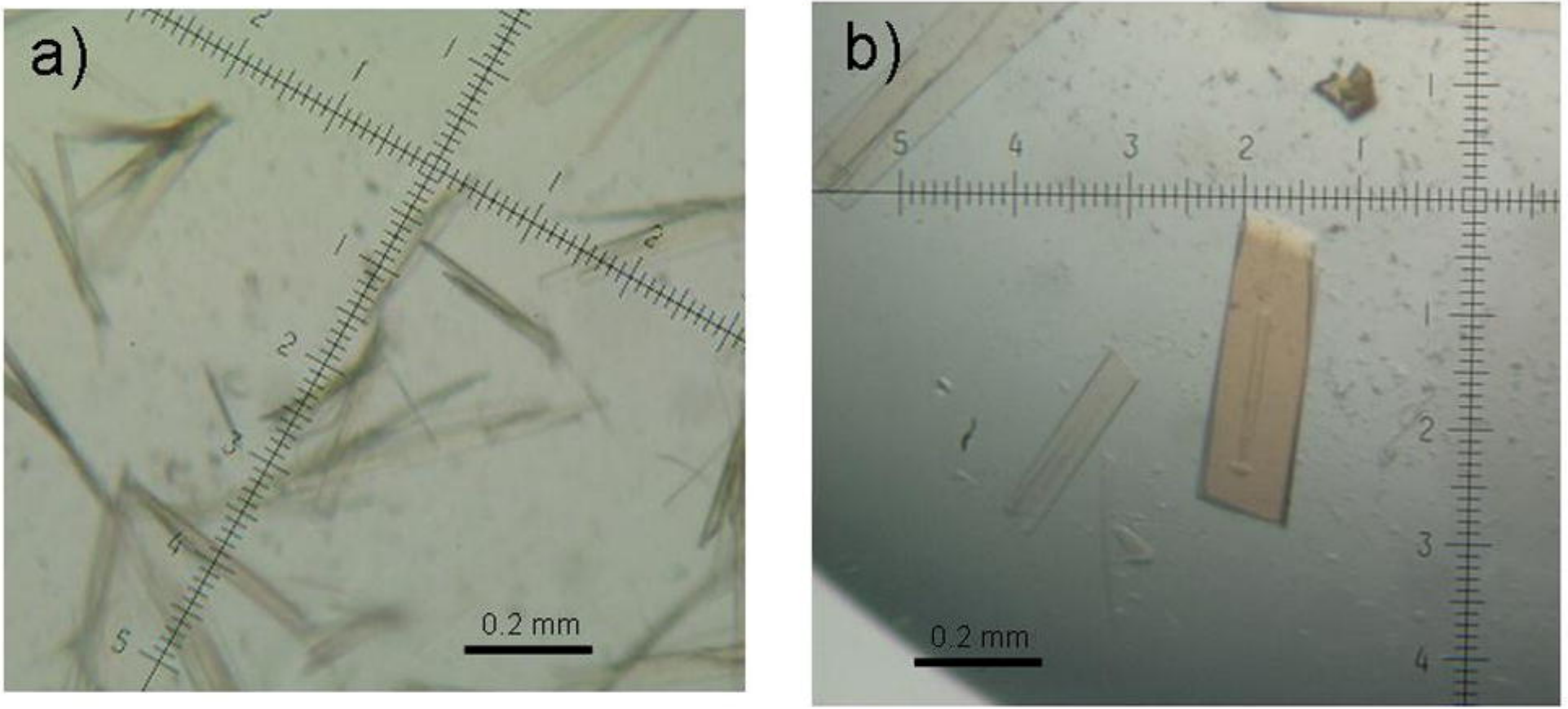

Figure 1

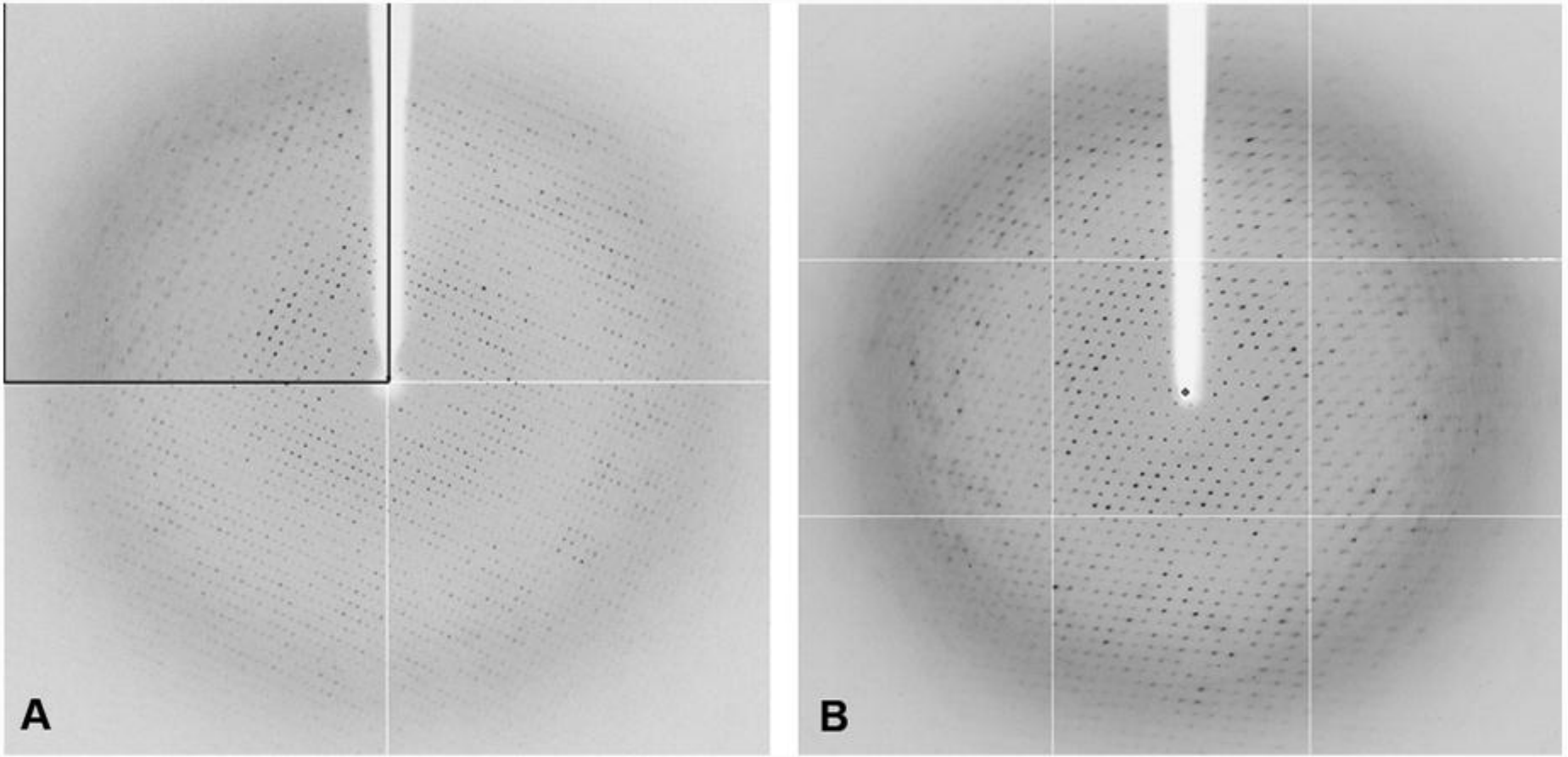

Figure 2

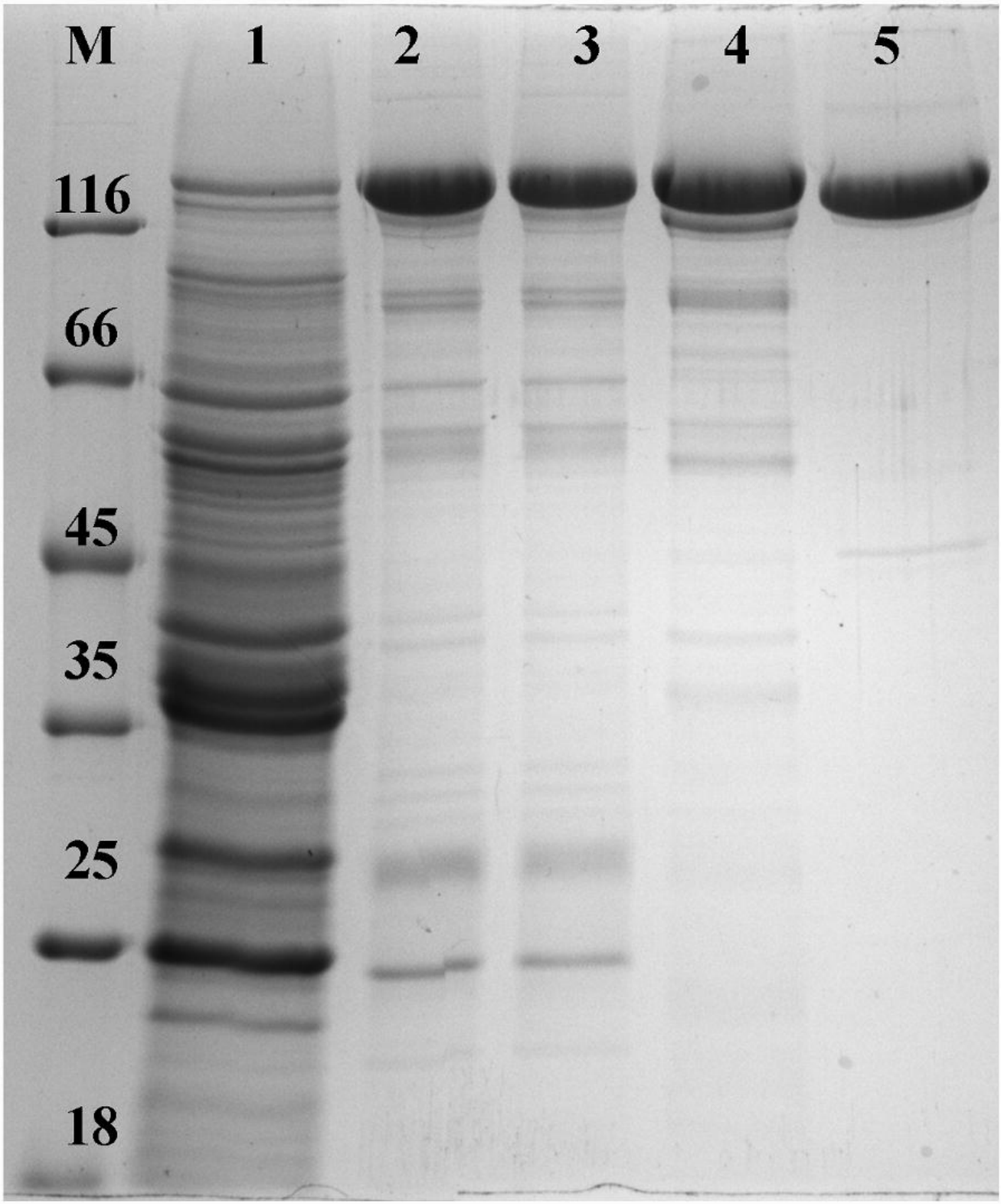

Figure 3

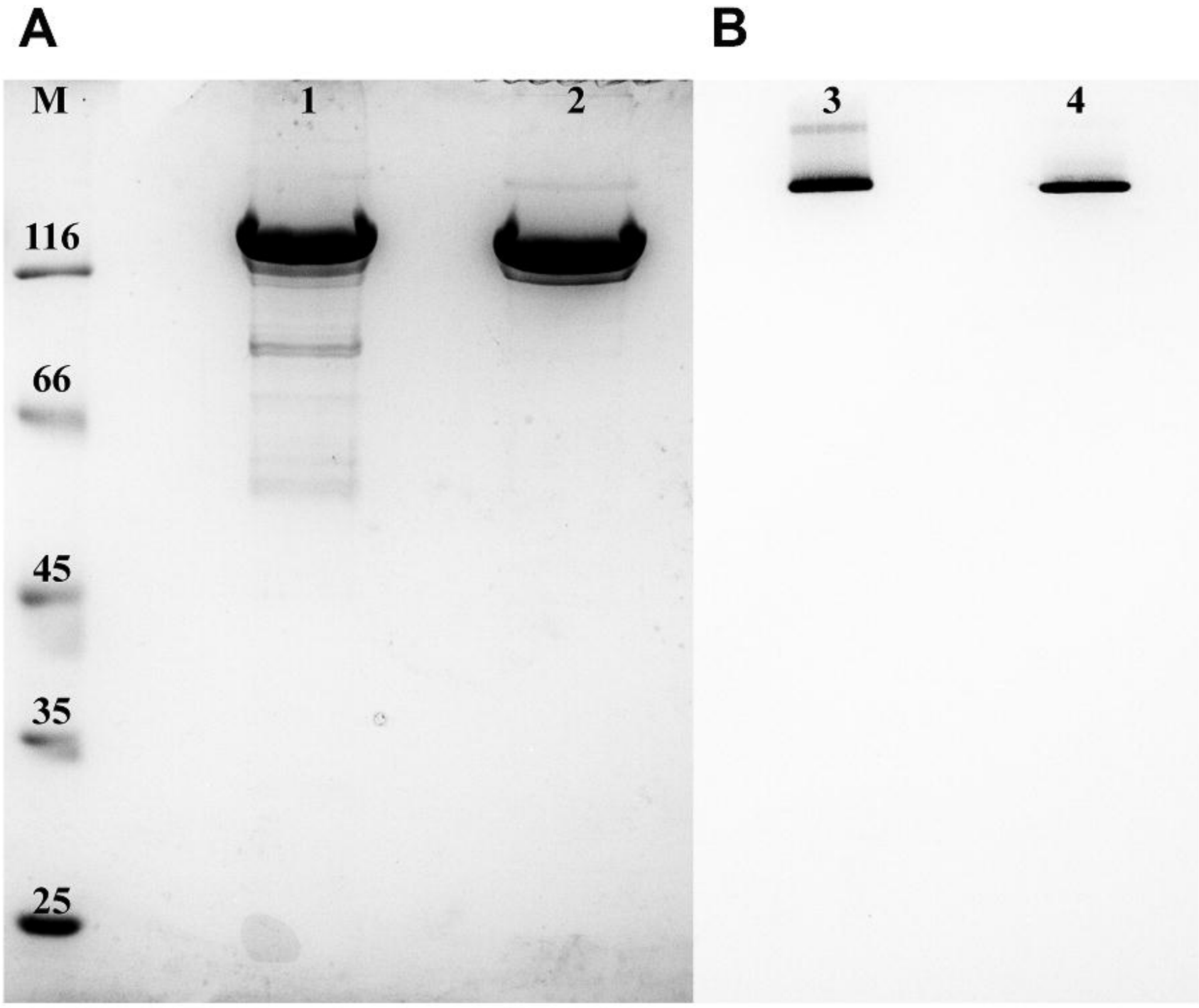

Figure 4

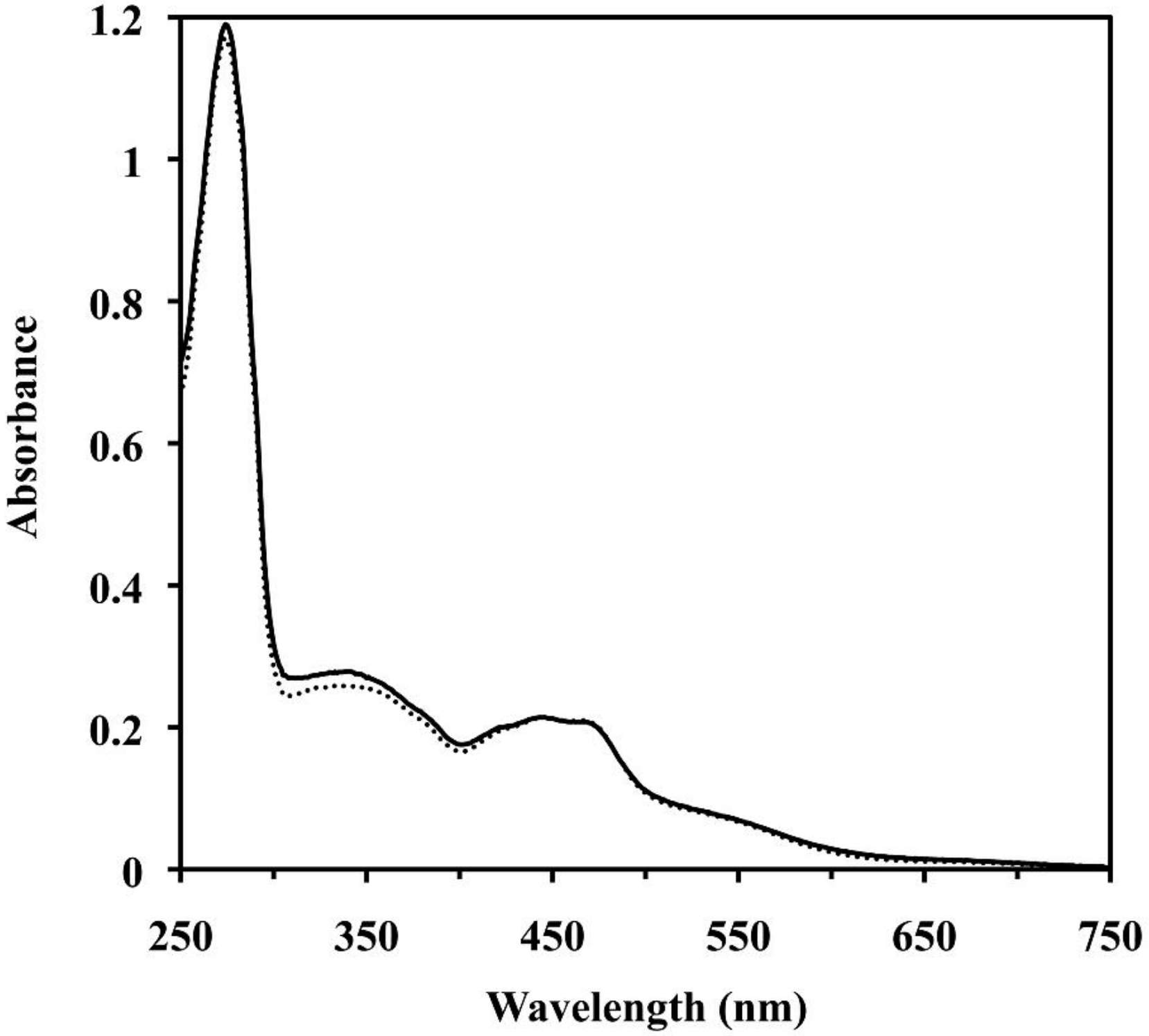
1.2
1
0.8
0.6
0.4
0.2
0
Absorbance
250
350
450
550
650
750
Wavelength (nm)

Figure 5

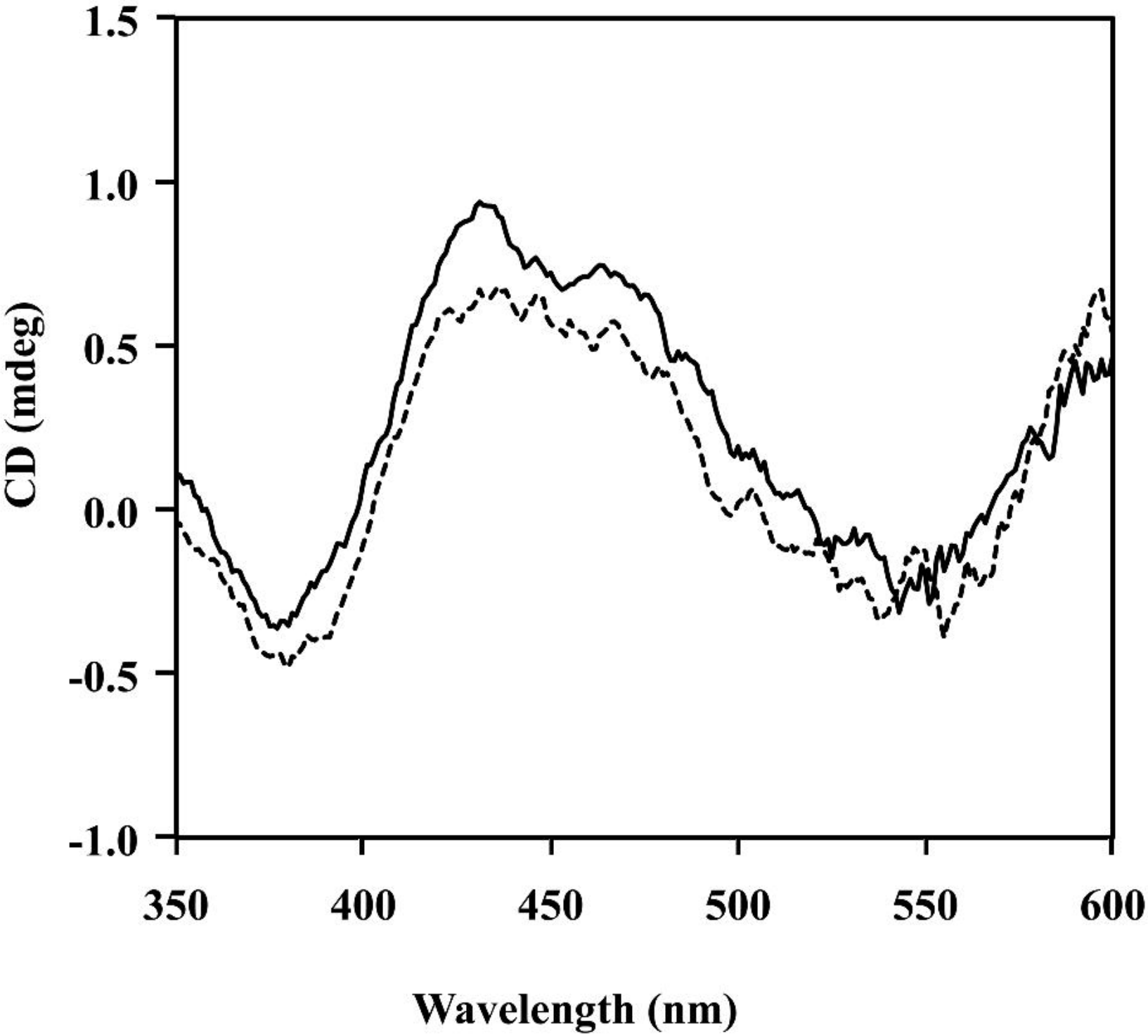

Figure 6

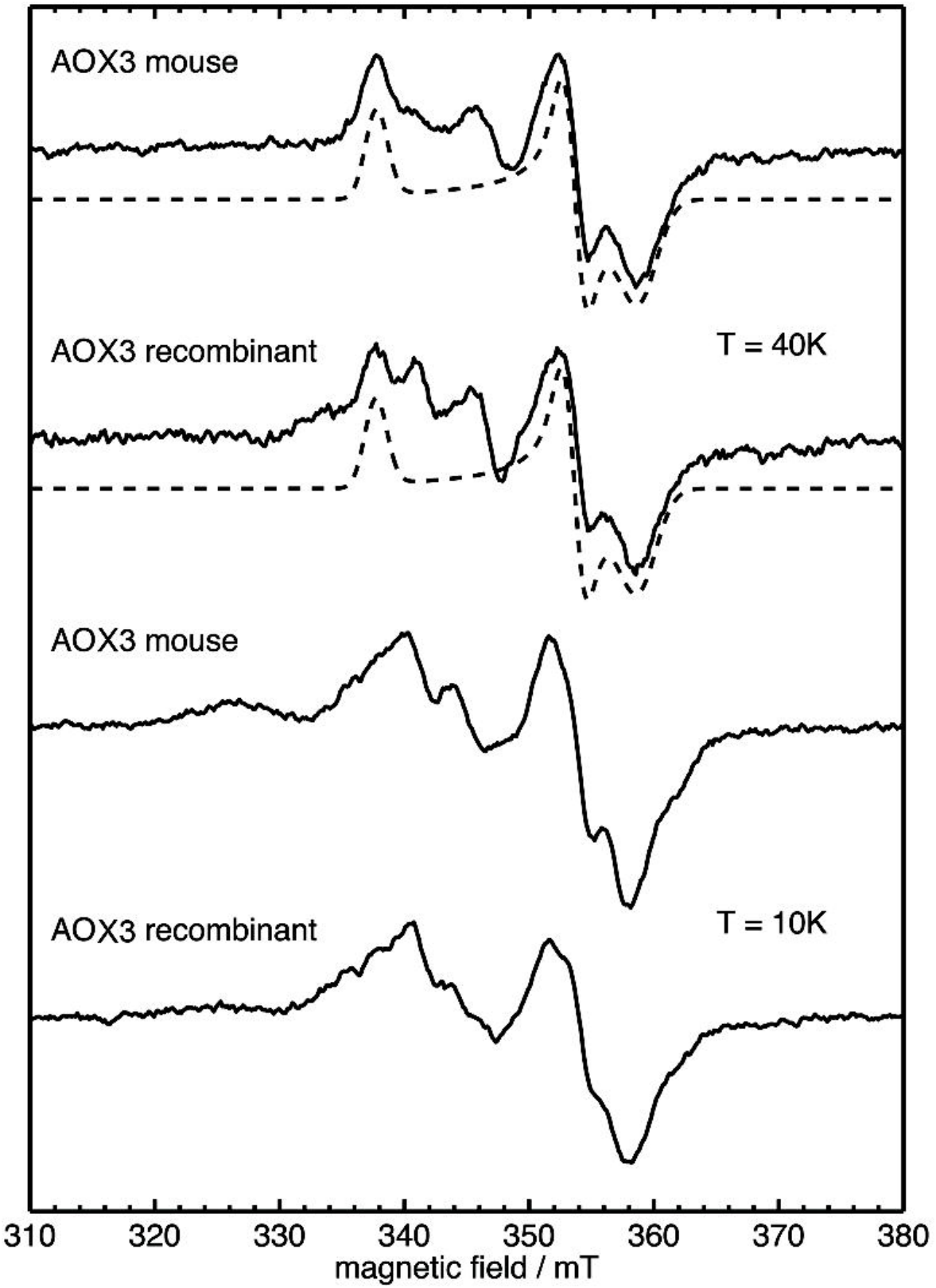
AOX3 mouse
AOX3 recombinant
T = 40K
AOX3 mouse
AOX3 recombinant
T = 10K
310
320
330
340
350
360
370
380
magnetic field / mT

Figure 7